Evaluating the influence of discharge depths of lithium-ion batteries on the mechanical recycling process

A. Kaas, C. Wilke, A. Vanderbruggen and U.A. Peuker

Abstract

During the discharge process of a lithium-ion battery different phenomena can occur, such as copper deposits or active material coating on the separator, which influence the quality of recycling. According to their depth of discharge the cell types investigated behave differently in the mechanical recycling. The product qualities of the black mass scatter regarding yield and content of impurities, which generates new challenges in terms of the required recycling rates according to EU regulations. plating on to the different structure of the components, the contamination of the black mass increases, while the liberation of active material is reduced. The findings of this study underscore the necessity of optimizing the mechanical recycling process to ensure stability in handling phenomena associated with greater discharge depths. Not addressing these issues would lead to the introduction of impurities that coat the separator, presenting new challenges for subsequence processes such as flotation and hydrometallurgy.

1. Introduction

Lithium-Ion Batteries (LIB) are an electrochemical storage system (Korthauer 2013) whose application has increased significantly over the last decade (Neef, Schmaltz et al. 2021). The functional unit of a LIB consists of two electrodes, cathode and anode, which are separated by a porous membrane, the separator foil. This unit is embedded in a casing and filled with electrolyte which enables the ion transport between the electrodes (Rothermel, Winter et al. 2018). The electrodes consist of a metallic current collector foil ensuring geometric stability and a coating (Sommerville, Shaw-Stewart et al. 2020). For the anode, copper (Cu) is used as current collector foil which is predominantly coated with graphite and fixed by carboxymethyl cellulose (CMC) and/or styrene-butadiene-rubber (SBR) as binder. The coating of the cathode is formed by a layered metal oxide containing different combinations of nickel, manganese, aluminium and cobalt or phosphate ($LiCoO_2$ (LCO), LiNixMnyCozO_2 (NMC), $Li_xMn_yO_z$, $LiNi_xCo_yAl_zO_2$ (NCA), $LiFePO_4$ (LFP)) (Korthauer 2013, Zhao, He et al. 2019). This active material is fixed on an aluminium current collector foil using predominantly polyvinylidene fluoride (PVDF) as binder. The separator foil prevents short circuits and is made of polyethylene or polypropylene or a mixture of both. To ensure further thermal stability the separator can be coated with inorganic materials like alumina and silica (Shi, Dai et al. 2016). The ion-conducting electrolyte consists of a conductive salt, most likely lithium

hexafluorophosphate ($LiPF_6$), and a mixture of organic solvents, i.e. organic carbonates (Doose, Mayer et al. 2021).

As LIB contain critical raw materials like Co, Ni and Li, a special economic and political need for recycling is essential to prevent material shortage of these materials. This need is especially pronounced as LIB are increasingly used to power electric transportation. The number of decommissioned LIB is expected to increase from 11 million in 2020 to 145-230 million worldwide in 2030 (Schmaltz 2023). To handle the shortage or criticality of materials and to enhance recycling efforts, the European legislation defined in 2023 element specific recycling rates. A recovery of 95% for Co, Cu, and Ni and 80% for Li by 2031 is proposed (EU 2023). China sets even higher recycling rates of 98 % for Ni, Co and Mg, 85 % for Li and 97 % for selected earths and other metals (Li, Yang et al. 2021). Due to this legislation, new challenges in LIB recycling arise as every step of the recycling chain has to be highly efficient and losses cannot be accepted. There are different ways to design the recycling process by combining variants of mechanical, hydrometallurgical and pyrometallurgical sub-processes. To find out more details about the process types, variants and their challenges, the authors refer to the following review articles (Sommerville, Shaw-Stewart et al. 2020, Werner, Peuker et al. 2020, Windisch-Kern, Gerold et al. 2022).

Prior to the recycling, almost all processes require discharging the LIB to prevent hazards such as ignition and explosions (Rothermel, Winter et al. 2018, Wuschke, Jäckel et al. 2019). However, during discharging further challenges occur, which derive from the depth of discharge. Following operation, cell interconnected in the battery pack can have different capacities. Discharging the cells connected in series with the same current can result not only in discharge and overdischarge of the cells, but also in reversal of the poles (Fuentevilla, Hendricks et al. 2015, Rothermel, Winter et al. 2018) of the cells with the lowest capacity in the pack. During overdischarging and discharging into pole reversal different phenomena can occur. Due to the voltage difference Cu ions from the anode current collector can be electrochemically dissolved and transported to the cathode side, where the Cu ions are reduced to metallic copper, which precipitates on the cathode active material (He, Liu et al. 2013, Kasnatscheew, Börner et al. 2017, Feng, Ouyang et al. 2018). This weakens the stability of the copper foil which starts to corrode (Hashimoto, Yamashiro et al. 2015, Rothermel, Winter et al. 2018). In addition to the formation of copper plating (Maleki and Howard 2006, Juarez-Robles, Jeevarajan et al. 2020), overdischarging acts on the separator foil, promoting the formation of copper bridges (dendrites) through the separator foil (Juarez-Robles, Jeevarajan et al. 2020). As a result, the adhesion of the active material to the porous membrane increases, since the precipitated copper acts a binder. Thus, the separator foil becomes coated with active material (Fear, Juarez-Robles et al. 2018, Hendricks, Mansour et al. 2020) and can even melt (Wu, Sun et al. 2015, Wang, Zheng et al. 2020) due to the heat generation resulting from

internal short circuit (Rothermel, Winter et al. 2018, Wu, Liu et al. 2018). Thus, the phenomena of deep discharge, especially internal short circuits, can also lead to thermal runaway. After a series of exothermic reactions, the thermal runaway leads to spontaneous ignition with a possible explosion (Doose, Mayer et al. 2021, Wang, Feng et al. 2023).

As the internal structure of the LIB changes with the depth of discharge, understanding how valuable materials can still be recovered becomes essential. It has already been proven that discharging has an influence on the intermediate product streams in mechanical recycling (Kaas, Wilke et al. 2023). When processing parameters are kept unchanged, the electrode product, e.g., after flow separation is contaminated by the coated separator and the black mass generated by sieving shows increased copper values for the pole reversed cells. However, the entire mechanical process is not analysed with regard to the recycling rates. Therefore, this study aims at quantifying how significant is the effect of, e.g., pole reversal on yield of certain regulation relevant elements. Furthermore, the already mentioned contamination of the black mass with copper can lead to problems in the subsequent processes like hydrometallurgy. During leaching, Cu^{2+} ions can co-precipitate with Co, Ni and Mn (Or, Gourley et al. 2020), necessitating, a multistage solvent extraction to remove copper impurities (Peng, Lahtinen et al. 2020) and enable a selective precipitation. If Cu is not removed from the black mass and the electrode materials are directly recycled, i.e. re-lithiated to build new cell, the impurities can cause short circuits (Park, Kim et al. 2019).

Due to the problems arising from impurities in recycling product streams, it is necessary to characterize how far the phenomena of overdischarge influence the mechanical recycling and the product streams generated. The recovery rates of specified elements like Ni, Co, Cu and Li serve as important metrics to evaluate the resilience of recycling processes under varying feed material properties such as the depth of discharge. However, currently, no study assesses the complete mechanical recycling process in this respect. For this reason, this study uses the material from (Kaas, Wilke et al. 2023) to evaluate the recycling products of the second part of the mechanical process chain (Wuschke 2018) and assesses the process carried out with regard to the prescribed recovery rates.

2. Materials and Methodology

The data behind the figures and additional data can be found in the supplementary information (Kaas, Wilke et al. 2024).

2.1 Material and methods

To evaluate a whole mechanical recycling process and the influence of the discharge level, four different battery types (P1, P2, P6 and C3) were investigated, which differ in geometry

and cell chemistry as shown in Table 1. The prismatic cells P1-P6 are classified by a NMC111 chemistry with different capacities whereas the cylindric cell C3 has LFP as cathode active material.

Table 1: Studied battery cells information, including their active materials and voltage after overdischarge and relaxation (PTC: positive temperature coefficient; IPR: into pole reversal)

Indication	**P6**	**P2**	**P1**	**C3**
Format	Prismatic	Prismatic	Prismatic	Cylindric
Capacity	94 Ah	20 Ah	n.a.	4 Ah
Chemistry	NMC111	NMC111	NMC111	LFP
PTC	0.44-0.49 V	0.76-0.82 V	0.32–0.44 V	1.29-1.63 V
IPR	0 V	0 V	0 V	0 V

The presented study used the material and data of (Kaas, Wilke et al. 2023). Therefore, the specific information about the discharge procedure can be found in (Kaas, Wilke et al. 2023). In summary, four cell types of the two different discharge levels: (a) positive temperature coefficient (PTC) and (b) into pole reversal (IPR). For the discharge level PTC the cells were discharged to a SoC < 0 % using an ohmic resistance. However, the residual voltage was far above 0 V. The IPR cells were discharged lower than 0V. This was done using a series connection of ohmic resistors and a battery with a higher residual voltage. The cells were investigated and the quality and yield of the recycling materials streams are quantified, discussed and compared to work out the effect of discharge.

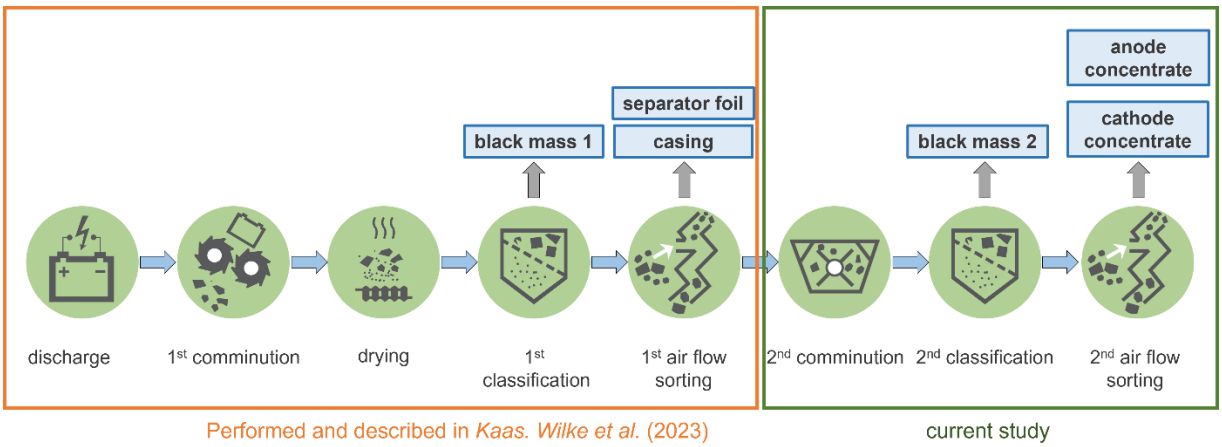

Figure 1: Recycling process of the LIB in (Kaas, Wilke et al. 2023) and the current study.

In this study the process of TU Bergakademie Freiberg (Wuschke 2018) was applied, schematically shown in Figure 1. In the first part of the process (Kaas, Wilke et al. 2023) the

final liberation of the LIB was performed by a fast rotating, single-shaft rotary shear (Universal Granulator UG300, Andritz MeWa GmbH; Gechingen, Germany) with a 20 mm discharge grid. Afterwards the crushed material was dried for 14 days at 22-25 °C. Black mass 1 is gained after the first classification of the dry material by sieving at 1000 µm. The electrode fraction is separated in the first air flow sorting at 2 m/s < v_s < 6.4 m/s. The separator fraction is gained at 2 m/s whereas the casing fraction was separated at 6.4 m/s. Now, the electrode fraction was subjected to a high impact mill (TurboRotor G-35S, MAHLTECHNIK GÖRGENS GmbH; Dormagen, Germany) to further decoat the electrode foils from the remaining active particles (both anode and cathode active material) and reshape them to more spherical particles. Afterwards a second screening using an EML 450 sieve machine (Haver & Boecker OHG; Oelde, Germany) at 500 µm removed the liberated coating generating black mass 2. The fraction larger than 500 µm is sorted by further air flow sorting step with a Zig-zag air classifier (ZZAC) (design of TU Bergakademie Freiberg, Germany) at 4.7 m/s air flow velocity into a cathode concentrate and an anode concentrate. To determine the composition of the individual product fractions, manual sorting was employed using tweezers.

To determine the cell composition, the cells were cut open, the jelly rolls enrolled and the casing, separator foil, anode and cathode foil collected separately. The materials were dried for 14 days at 22-25 °C. The mass difference was determined as electrolyte mass. Defined mass of the separator foil, cathode and anode were dissolved by microwave digestion and then analysed by ICP-OES, just like the black mass later on. This made it possible to determine the masses of Li, Co, Mn and Ni contained in the battery. The masses of copper and aluminium obtained were compared with those from the dismantling of the casing. Therefore, the determination of the masses for the metals Cu, Li, Co and Ni, which are relevant for the required recycling rates is possible.

The content of Co, Cu, Fe, Li, Mn, Ni and P in the black mass was determined by digesting with inverse aqua regia in a Multiwave 7000 (Anton Paar GmbH; Graz, Austria). The solution was analysed with Inductively Coupled Plasma Optical Emission Spectroscopy (ICP-OES) (iCAP 6300, Thermo Fisher Scientific Inc; Waltham, United States). Additionally, the black mass was analysed by Scanning Electron Microscopy (SEM) (FEI 30 ESEM-FEG; FEI Europe B.V.; Eindhoven, Netherlands) with HighVac mode. For detailed optical image analysis of the separator foil, an optical microscope (LiMi Zeiss AxioLab A1) was used. The coated separator foil underwent pyrolysis using a pyrolysis tube HTR11075-230SN (Carbolite Gero GmbH; Neuhausen, Germany) under nitrogen atmosphere at 450°C. Afterwards the pyrolysis product was analysed by SEM (FEI Quanta 600 F) equipped with a field emission source (FEG) and an SSD-EDS X-ray spectrometer (Bruker Quantax X-Flash 5030 EDS-Detectors). The loose powder samples were fixed on a tab (PELCO Tabs TM, 6 mm OD from TED PELLA, INC, Redding, CA, USA). To evaluate the structure of the copper current collector foil of P6 for PTC

and IPR, Atomic Force Microscopy (AFM) with a Cantilever (ContAl-G von BudgetSensors, Bulgaria) was applied using the AFM XE-100 by Park Systems Europe GmbH (South Korea). For further details to the C-AFM measurements, refer to (Gräfensteiner, Friebel et al. 2024). In the present study, a scan size of 20 µm with a scan frequency of 0.7 Hz and a set point of 7.0 nN was applied.

2.2 Calculations

The used symbols and indices of the publication can be found at the end of the publication.

To calculate the mass fraction (w_i) of the different components within the products (electrode product before and after second crushing, anode and cathode concentrate), Equation 1 was applied. Here, the mass of the individual component ($m_{Component}$) was divided by the total mass of the product (m_{Total}).

$$w_i = \frac{m_{Component}}{m_{Total}} \quad (1)$$

Using Equation 2 it was possible to calculate the component recovery (R_c) into the different products for a process. Therefore, the mass of the component in the product ($m_{i,Product}$) was divided by the mass of the component in the feed of the process ($m_{i,Feed}$).

$$R_c = \frac{m_{i,Product}}{m_{i,Feed}} \quad (2)$$

For example, regarding the overall copper recovery ($R_{c,Cu}$) the sum of the mass of copper ($m_{Cu,product}$) in the different products casing, black mass and anode concentrate were related to the total mass of copper (m_{total}) in the cell.

$$R_{c,Cu} = \frac{\sum m_{Cu,product}}{m_{Cu,total}} \quad (3)$$

In the case of copper, which is specified in the EU regulation (EU 2023), there are different sources in the initial battery, which contribute in addition to the anode foil to the overall copper content. Since the copper shows different appearance in the battery cell, e.g., foil, compact part, wire, the copper will end up in different recycling streams using the established process scheme discussed here.

The black mass yield (Y_{BM}) was obtained using Equation 4 by dividing the mass of the produced fraction (m_{BM}), for black mass 1 (< 1000 µm) and for black mass 2 (< 500 µm), by the cell mass (m_{Cell}).

$$Y_{BM} = \frac{m_{BM}}{m_{Cell}} \tag{4}$$

The maximal archivable black mass yield ($Y_{BM,\ maximal}$) was calculated by dividing the mass of coating ($m_{coating}$) by the cell mass (m_{cell}).

$$Y_{BM,maximal} = \frac{m_{Coating}}{m_{Cell}} \tag{5}$$

The metal recovery (R_{Me}) was calculated for Co, Li and Ni and compared to the specifications of the European legislation for the recycling efficiencies in 2031 (EU 2023) by Equation 6. Therefore, the mass of the respective metal in the black mass ($m_{BM,Me}$) was related to the mass of the respective metal in the cell ($m_{cell,Me}$). The masses were calculated from the measured metal concentration in the black mass ($c_{BM,Me}$) and in the whole cell ($c_{Cell,Me}$) by Equations 7 and 8.

$$R_{Me} = \frac{m_{BM} \cdot c_{BM,Me}}{m_{cell} \cdot c_{Cell,Me}} \; with \; Me = Co, Li, Ni \tag{6}$$

$$c_{BM,Me} = \frac{m_{BM,Me}}{m_{BM}} \tag{7}$$

$$c_{Cell,Me} = \frac{m_{Cell,Me}}{m_{cell}} \tag{8}$$

The metal oxides (MeO) are defined for the NMC chemistry as Ni, Co and Mn whereas for the LFP chemistry a MeP is defined with the metal oxides Fe and P. Li was not added as contribution to the metal oxide or metal phosphate as it can be contained in the LiMeO and LiMeP as well as in the conductive salt. Therefore, the abbreviations MeO and for the LFP active material MeP were introduced. The MeO was calculated for the cathode active material NMC by assuming the stoichiometric ratio to be 1:1 between Me and O_2. Hence, the contribution of O_2 was mathematically added to the measured Co, Mn and Ni contents. For the calculation of the MeP content only Fe was used as P can derive from both LFP and $LiPF_6$.

Small contamination amounts of Fe from the processing machines were neglected and also counted as Fe from the LFP.

To obtain the yield of metals in the black mass ($Y_{BM,Me}$) for MeP, MeO and Cu, the measured concentration of the respective metal ($c_{BM,Me}$) was multiplied by the according yield of black mass (Y_{BM}).

$$Y_{BM,Me} = c_{BM,Me} \cdot Y_{BM} \quad (9)$$

To calculate the degree of liberation *E*, the mass share of compounds in the recycling streams was determined. The overall liberation was calculated by taken both crushing steps into account.

$$E = 100 - \frac{m_{compounds}}{m_{cell}} \quad (10)$$

As compounds are counted particles which macroscopy still attached to each other, e.g., separator to electrode foils or thinner plastics to separator foil. Coated separator foil and electrodes with remaining coating are not characterised as compounds.

3. Results and Discussion

3.1 Degree of liberation

Liberation is one of the most relevant parameters in a recycling process. Since the separation properties required for sorting can only be utilised on liberated particles. The limited de-coating of the IPR cells results from the generation of new compounds of the cathode active material and the separator foil. Due to the Cu-plating the bonding of separator foil to the coating increases, with simultaneous adhesion of the active material to the cathode foil more compounds remain after the mechanical stressing. This is supported by the formation of dendrites at the separator (Hendricks, Mansour et al. 2020, Flügel, Kasper et al. 2021) leading to higher cohesion. The difference in total liberation in the process chain is largely attributed to the compounds transferred to the casing material fraction in the first stage of the process chain (Kaas, Wilke et al. 2023). Here, larger coated separator particles are generated during 1st comminution, which in 1st classification go along with thin plastic particles and electrodes. The stress during the second crushing ranges between 8.2 kWh/t (P6-IPR) and 14 kWh/t (C3-PTC). For more detailed information please have a look at (Kaas, Wilke et al. 2024). The compounds from the first stage, which were transferred to the electrode fraction, are liberated to nearly 100% in the second crushing and therefore do not affect the overall black mass yield. The total degree of liberation *E* of PTC cells ranges from 98% (C3) to 99.9% (P6) (Kaas, Wilke

et al. 2024). In general, the IPR cells had a minor degree of liberation than the PTC cells. As the IPR cells contain coated separator foil, due to the higher adhesion of components, the liberation is minor within a range of E = 94% (P2) and E = 97.3% (P6). As highlighted by (Kaas, Wilke et al. 2023), P2 showed the highest proportion of coated separator, indicating higher bonding of components to the separator foil than in other IPR cells. The remaining compounds after the second crushing are characterized as elongated, thin plastic foils, originating from the inlay foil of the casing, with coated separator. Due to the elongated shape of the compound particles and the strong bonding within the compound, even the high impact stress in the second comminution step may not be sufficient for liberation. Nonetheless, since these compound particles constitute a minority and the liberation of the other compounds, e.g. electrode foils with remaining active material in the second crusher is nearly perfect, the second comminution stage can be regarded as ideal for the material in terms of liberation. The decoating behaviour of the electrodes, as well as the bonding mechanisms of the composites and the coatings on the foils, e.g. cathode coating on separator foil should be investigated more. The types of bonding mechanisms as well as the strength of adhesion should be investigated, e.g. by means of peel-off tests. These tests can also provide information on the decoating behaviour and the strength and type of stress to be applied. An earlier integration of the high impact stress should be investigated in order to examine the damage of the crushing tools, considering that not all mill types are suitable for stronger casing materials. Additionally, it could potentially increase the content of iron impurities in the fine black mass fraction.

3.2 Change of composition

Alongside with the liberation of compounds, the second crushing is applied to further decoating of the electrodes. Therefore, it is expected, that the share of coating material in the product increases. This trend is supported by the results shown in Figure 2a. For the PTC as well as the IPR cells, the total proportion of electrode and coating increases, which are the desired products of the mechanical recycling. Especially for the P2 IPR a growth of 25% (from $w_{\text{coating,before}}$ = 35% to $w_{\text{coating,after}}$ = 60%) and C3 IPR of 29% (from 57% to 86%) is achieved. These two types can be used to explain the reason for the increase. For the C3 IPR the share of compounds in the electrode product was the greatest among the investigated cells with $w_{\text{compounds,before}}$ = 37%. Those compounds are liberated during the second crushing and their share minimized to 0.6%, resulting in a rise of coated separator foil and electrodes, as depicted in in Figure 2b. In the case of C3 IPR, the mass of coated separator foil doubled, which is due to the liberation of compounds, since these contain the separator. Additionally, to the liberation of compounds, a partial decoating of the coated separator foil occurred in parallel, resulting in a decrease of coated separator foil while the proportion share of coating increased. For P2,

the mass fraction of coated separator is decreased from 55% to 31%, while the combined mass fraction of electrode and coating increased from 35% to 60%. These values are still very high, trapping the target material coating material in a compound. In the case of P6, the most significant decrease in the mass of coated separator was observed with -79% (Fig. 2b) and illustrated in Figure 2c. The composition analysis of the feed and product of the crusher shows that the share of coated separator decreased for P6 from 6.8% to 1.8%. In case of P2, the massive coating of the separator foil led to a significant proportion of this component in the electrode product after sifting (Fig. 2a). However, due to the high impact mill, the proportion could be reduced from 54.9% to 31.4%.

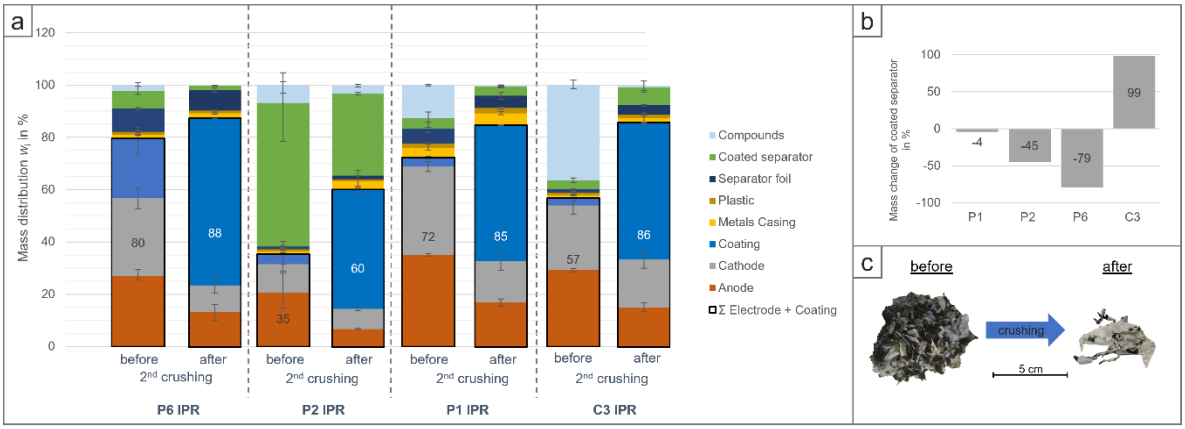

Figure 2: (a) Change of the composition of the electrode product before and after the second crushing, with the change of mass (b) and appearance (c) of the coated separator foil after the second crushing of sample P6. The values in 2a state the combined share of electrodes and liberated coating.

However, the question arises as to whether the coating of the separator film consists only of cathode active material or also contains other components like, for example, copper. To find this out, a detailed microscope image of the coated separator foil of P6 IPR was taken (Fig. 3a). Notably, distinct regions in black, as observed in Fig 2.c, were identified as cathode active materials. In addition, during the discharging into pole reversal copper bridges are formed (Juarez-Robles, Jeevarajan et al. 2020) through the separator foil and metallic copper is finally deposited onto cathode foil, which becomes visible in Figure 3a as bright red particles. This statement is also supported by the local position of the copper layer. The copper is deposited directly onto the separator in between the separator surface and cathode active material. To corroborate these observations, SEM-EDX imaging (Fig. 3b) was employed to ensure that the phases to be seen are cathode active material and copper. Before conducting the recording of the SEM image, the separator underwent pyrolysis to mitigate potential interference from plastic constituents with the electron beam, thereby ensuring precise characterization of the coating material.

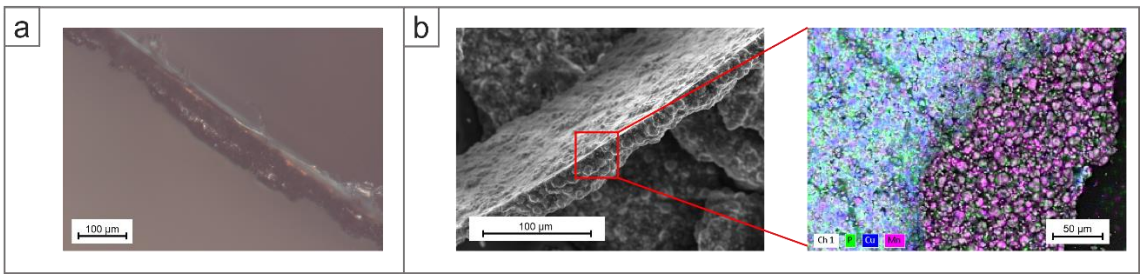

Figure 3: (a) Coated separator foil of P6 recorded with light microscope and (b) pyrolysed coating of the separator foil recorded via SEM.

The pyrolyzed particles remained stable and revealed a plate-like form, as observed in Figure 3b. The EDX analysis confirmed that the flat side of the particles originating from the contact with the separator corresponds to the copper phase, while the particles of the NMC cathode material are forming the irregularly shaped layer on top of it (Fig. 3b). This confirms the assumption of copper dendrite formation on the separator. Additionally, despite the intense stress exerted during the crushing sand milling steps during mechanical processing, the separation of copper and NMC particles was unfeasible, indicating a strong interlayer bond. Analysis of the powder after the pyrolysis treatment shows a Cu concentration of 21% and a NMC concentration of 65%, underscoring the necessity of recovery of the coating through further processing. One viable approach involves the previously implemented pyrolysis method, while another option entails acid leaching of the separator foil to dissolve the metals from the coating layer.

3.3 Copper recovery

The copper recovery is one part of the new European battery legislation (EU 2023), which mandates a 95% recovery rate of copper in LIB by 2031 For the process carried out in this study, copper recovery was categorised in the respective process streams: casing, anode concentrate and black mass (Fig. 4), thus there is no specific copper concentrate generated. First, depending on the thickness copper foil used in the design of cell such as the nail safety device and current collector foil, the copper can be transferred to different process streams. More detailed information about the design of the investigated cells and their components can be found in (Wilke, Kaas et al. 2023), wherein the varying shares of copper transferred to the casing are elucidated. Notably, C3 cells have a small amount of thicker copper components, whereas prismatic cells are equipped with an additional nail safety device made of a stronger copper foil. However, the main difference in the copper recovery concerning the different depths of discharge is not evident in the casing fractions but rather for the anode product and the black mass. Specifically, for P1, no variation in copper recovery was determined. In the case of C3, the IPR cell shows an even greater proportion of copper recovery within the anode concentrate. One possible reason is the different transfer of the greater anode current collector

particles to either casing or anode concentrate earlier in the process scheme. Given that the particle size is proportional to the settling velocity, larger particles of the anode current collector may be preferentially transferred to the casing fraction during the first air flow sorting process.

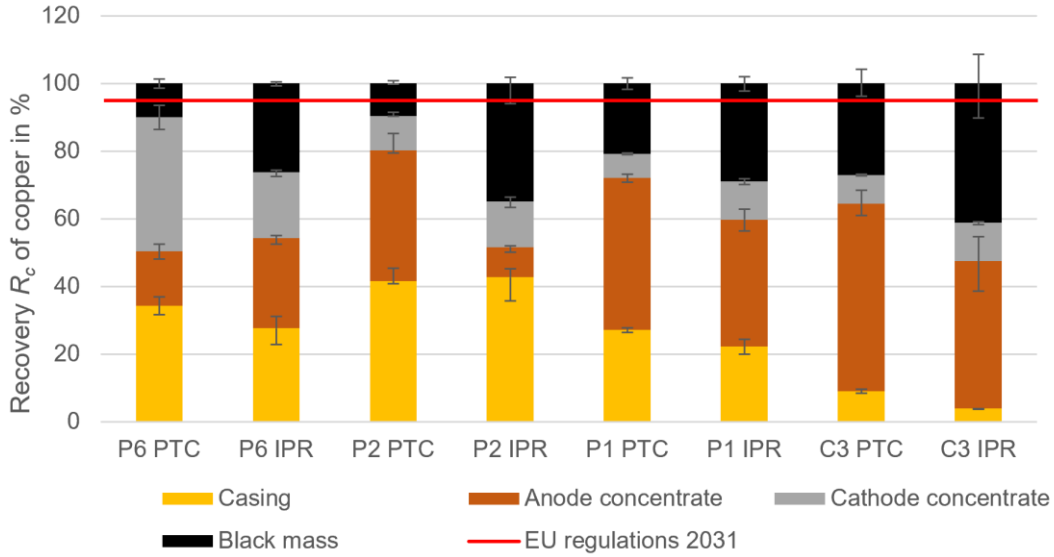

Figure 4: Recovery of copper to the fractions casing, black mass as well as cathode and anode concentrate compared to the target of the EU legislation (red line) for the investigated cells and discharge levels.

Comparing the different discharge levels of P2, it can be observed, that the recovery of Cu to the anode concentrate is marginal for the IPR to the PTC cells while having an equal recovery share to the casing. As a consequence, for P2, more copper is recovered into the black mass for the IPR discharge level since it sticks to the cathode material. Thus, the proportion of copper transferred to the cathode concentrate is higher for the IPR cell. The same occurs for P1 and C3. This phenomenon can be additionally explained by the weakened current collector foil, which broken down into smaller particles with reduced settling velocity. Thus, the copper particles are sorted to the light fraction of the ZZAC separation. Among the prismatic cells, P2 shows the highest recovery of Cu into the black mass with $R_{c,Cu}$ = 34% (Fig. 4). The transfer of the Cu to the black mass is reasonable, as the cathode coating is coated with metallic copper due to the discharge into pole reversal (Kasnatscheew, Börner et al. 2017). Furthermore, the partial decoating of the coated separator during the second comminution step contributes to an additional increase in copper recovery to the black mass fraction. However, this distinct trend is predominantly observable in prismatic cells. In the case of P6, a higher copper recovery to the casing is notable for the PTC cell, possibly attributed to the greater comminution of IPR anode foils due to the corrosion of the cells (Kaas, Wilke et al. 2023). Therefore, smaller particles are generated, which are better sorted to the electrode fraction in the first air flow sorting due to their low settling velocity. In contrast, larger anode particles of the PTC are transferred to the casing fraction. However, another consequence of the corrosion

of the anode foil for the PIR cell is the easier break down in the second comminution step. Thus, finer particles are generated and end up in the black mass whereas other smaller parts are still transferred to the anode product.

In regard of the P6 PTC, larger delaminated anode particles are transferred to the casing fraction. For C3 and P1, the recovery of copper to the black mass differs only slightly. This can be explained by the minor copper deposits on the cathode active material. As a result, during decoating, less copper is transferred to the black mass. However, none of the investigated cells meet the required recovery rate for copper if only the fractions casing and anode concentrate are considered. Therefore, establishing further treatment of the black mass concerning Cu recovery is imperative. An alternative could involve a milder stress to the electrode fraction during the second crushing. However, this might result in insufficient decoating. Another possibility is to vary the cut size for the black mass separation to limit the impurities as already proclaimed by (Wilke, Werner et al. 2023). Nonetheless, reducing the amount of copper in the black mass is feasible, but separating copper particles from the active material remains unattainable.

The significant transfer of copper to the black mass fraction of the IPR cells due to the coating of the cathode, a closer look to the properties of feed material current collector foil is necessary. As already stated in literature (Maleki and Howard 2006, He, Liu et al. 2013), the copper is ionized and transferred to the other electrode. Hence, a distinct structure of the copper current collector foil for PTC and IPR cells is expected. To confirm the assumption of ion migration from the anode to the active material of the cathode, samples of both PTC and IPR current collector foil were taken at different points of the anode. Uncrushed cells corresponding to their respective discharge levels were selected for this purpose. The copper foil was still partially coated. The graphite coating was removed with the aid of water. The obtained foil pieces with a defined area were afterwards weighed. The distinction of PTC and IPR anode is visually evident, as illustrated in Figure 5a, where the copper current collector foil of the PTC cell exhibits a familiar metallic shine, whereas the foil of the IPR cell appears brownish matt. It can be assumed that corrosion (Hashimoto, Yamashiro et al. 2015, Rothermel, Winter et al. 2018) of the copper has occurred due to the depth of discharge.

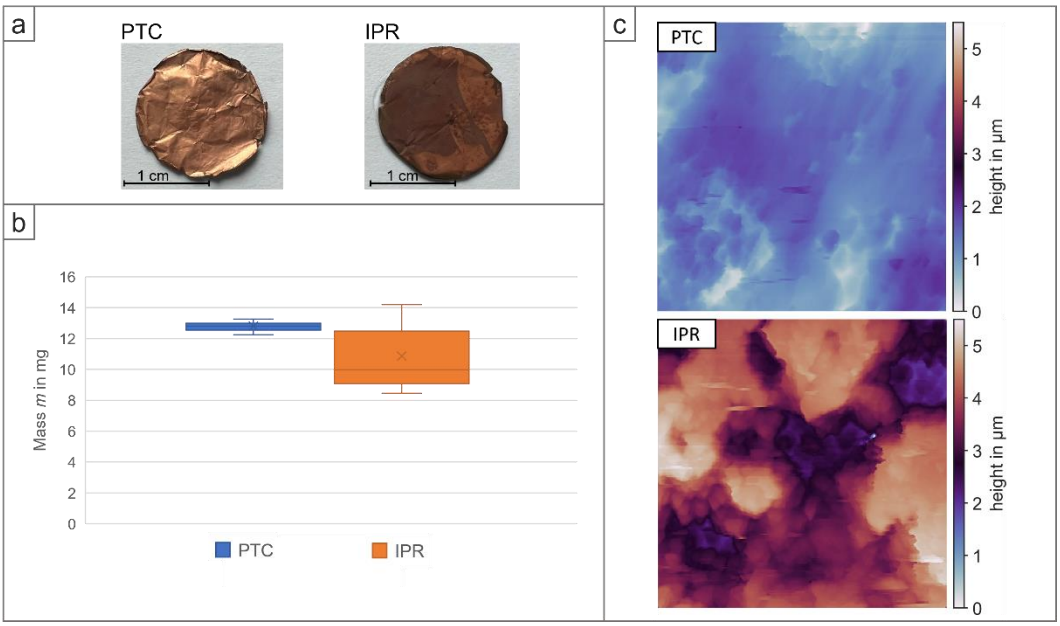

Figure 5: Difference of the anode current collector of P6 for the discharge levels PTC and IPR concerning their (a) macroscopic, (b) mass distribution and (c) morphology (AFM image).

As depicted in Figure 5b, the distribution of the weight of 25 pieces each of PTC and IPR copper current collector foil. The weight distribution of PTC cells ranged consistently between 12.25 mg and 13.26 mg, suggesting minimal fluctuations in mass. Conversely, 50% of the masses of the IPR samples ranged from 9.06 mg to 12.48 mg, indicating notable variability. This discrepancy confirms that the samples from PTC cells exhibit minimal structural changes, a finding supported by AFM measurements (Fig. 5c). The copper foils of the PTC cell analysed are very similar in structure to freshly produced copper foils by rolling processes (Yung, Wang et al. 2007, Xiao, Kim et al. 2013) showing a very small roughness. In contrast, the structure of the IPR cells displays completely different characteristics. As illustrated in Figure 5c, the sample exhibits an irregular surface structure, characterized by an increased number of peaks and valleys. This confirms the corrosions originating form release of copper ions and thus the altered and rough structure of the current collector foil. The pronounced fluctuations in the mass of the samples indicate a distribution of the weak points over the entire anode. In some areas the foil is intact, while in others significant degradation of the current conducting foil through ion migration is observed. The weakening of the structure due to discharge up to pole reversal can also lead to an increased share of fine copper in the black mass. At the same time, there is a reduced copper recovery to the anode concentrate.

3.4 Black mass

The black mass was subjected to a comprehensive analysis using the data from (Kaas, Wilke et al. 2023) alongside the results of the second stage of the process (Fig. 1) carried out. First of all, a mass balance compares the actual yield of the black mass to the maximal yield,

calculated from the mass of coating, both anode and cathode, in the cell. Here, all investigated batteries behaved differently. In Figure 6a, it is noticeable that the yield of P1 even exceeds what is theoretically possible. The latter has to be attributed to impurities within the black mass fraction. However, the extent to which the PTC cell exceeds the theoretical yield is comparatively less pronounced. According to the literature, impurities derive from the crushing and comminution steps (Wilke, Werner et al. 2023), since small particles of electrode foils and some casing materials are generated which end up in the black mass after sieving.

As copper, in addition to the usual amount of impurities, increasingly spreads into the black mass due to the effects during overdischarge, it is shown additionally in Figure 6a. As can be seen in Figure 6a for P1, the higher copper contamination in the IPR cell causes the higher overall yield of the black mass. In general, a comparison across all cell types with regard to the discharge depths shows that the IPR cell has generally a higher copper contamination. As already mentioned, this results from the copper plating on the cathode, which is connected to the decoating of the coated separator. Furthermore, all cells showed a further increase in copper contamination due to the mechanical processing in second stage, which can be caused by the higher stress in the second comminution step. On the one hand, the higher stress is required to achieve the de-coating of the cathode, which is results in a higher share of MeO/MeP in black mass 2. On the other hand, the current collector foils are subjected to a higher stress and therefore can break down to smaller particles. As a result, those end up as impurity in the black mass. The likelihood of copper foils breaking more easily in IPR cells is even higher due to pre-existing damage from discharge into pole reversal, as depicted in Figure 5b and corroborated by literature Figure 5a (Hashimoto, Yamashiro et al. 2015). However, the adhesion of the plated copper to the cathode active material seems to be significant, as mechanical detachment from the cathode particles is not feasible. Figure 6b presents a SEM-EDX image of a NMC agglomerate still carrying significant amounts of Cu plating.

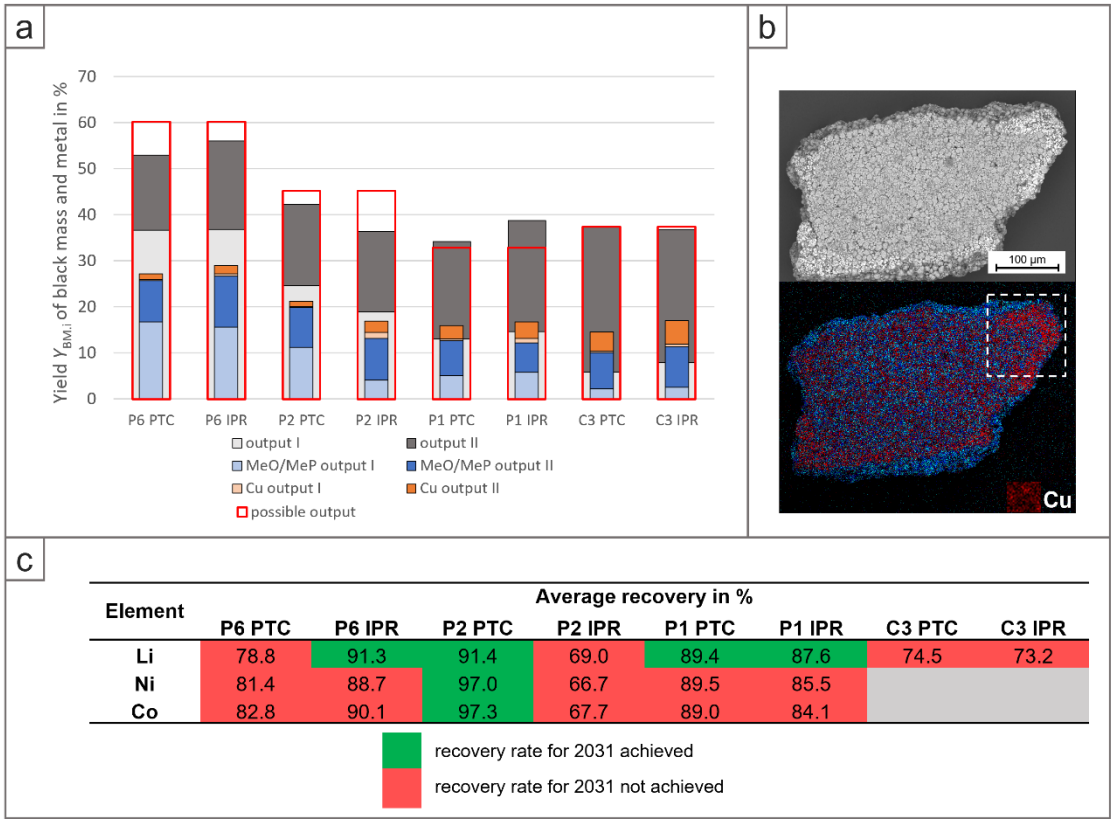

Element	Average recovery in %							
	P6 PTC	P6 IPR	P2 PTC	P2 IPR	P1 PTC	P1 IPR	C3 PTC	C3 IPR
Li	78.8	91.3	91.4	69.0	89.4	87.6	74.5	73.2
Ni	81.4	88.7	97.0	66.7	89.5	85.5		
Co	82.8	90.1	97.3	67.7	89.0	84.1		

recovery rate for 2031 achieved
recovery rate for 2031 not achieved

Figure 6: Analysis of the total black mass for the investigated cells and discharge levels concerning their (a) yield of black mass, yield of copper and yield of MeO/MeP for the first and second classification, (b) composition of a black mass particles recorded by SEM-EDX and (c) recovery rates of Li, Ni and Co compared to the EU legislations targets for 2031.

Focussing again on the yield of black mass, P2 shows like P1 a difference concerning the discharge levels. The minor yield of P2 for the IPR level is explained by the great plating of cathode active material on the separator foil. Therefore, less coating can be transferred to the black mass fraction. This is underlined by the great amount of coated separator foil in the electrode product with a share of $w_{coatedseparator,after}$ = 32% (Fig. 2a). In contrast, both discharge levels of C3 cells generate similar yield of black mass, although the IPR cell contains more copper due to plating, even though to a lesser extent than observed in P2, as previously demonstrated by (Kaas, Wilke et al. 2023). In addition, the decoating of the cathode foil was not sufficient for both discharge levels when comparing the decoated particles of C3 to the particles of the other cell types by visual observation. This results in a minor yield of MeP in the black mass. It is likely that the higher yield of black mass originates from the contribution of impurities e.g., copper like for P1 IPR to the overall mass collected. This is supported by the data on the copper recovery displayed in Figure 4. Regarding P6, the IPR cell shows like P1 a higher yield compared to the PTC cell. This results from a greater share of copper in the black mass, as more copper is recovered to the black mass (Fig.4). However, the black mass of the IPR cell contains also slightly (1%) more MeO. In combination with the greater yield a higher recovery of around 7% of Li, Ni and Co is reached for the IPR discharge level as can be seen

in Figure 6c. With the exception of P6, all cell types demonstrate better recoveries of the elements specified in the new EU legislation at the PTC discharge level. One potential explanation for P6 could be attributed to the improved recovery of MeO, facilitated by the effective decoating of the coated separator foil for IPR (Fig. 2b). Conversely, the inferior decoating of cathode particles is responsible for the comparatively lower Li recovery observed in the C3 cell. With the exception of P2 IPR, P6 PTC and C3, the Li recovery rate of 80% which is prescribed in 2031 by the EU could be reached. The recovery rates of Li, Co, and Ni are similar to each other due to the stoichiometric ratio of Li to MeO. Hence, it can be concluded that by achieving the recovery rates of Co and Ni, Li recovery into the black is also attained. The Li has to be separated in further, e.g. hydrometallurgical steps, from the MeO particles (Wang, Chen et al. 2019, Zhao, Zhang et al. 2019).

However, the poorest recovery rates were observed in P2 IPR. This can be attributed to the extensive transfer of coating to the separator foil product as well the minor decoating of them compared to the P6 IPR (Fig. 2b). In summary, it is important to control the depth of discharge in order prevent overdischarge and with it a massive copper coating of the separator foil. When the separator cannot be decoated sufficiently, the recovery rates in the established mechanical processes become more challenging.

Additionally, it has to be kept in mind that with a greater depth of discharge more impurities are transferred to the black mass such as copper. This can greatly affect further processing steps like hydrometallurgy in terms of consumption of chemicals. Therefore, it is recommended to further investigate the fractions of the black mass where impurities are present and assess whether it is possible to adjust the cut size for black mass separation to come to better qualities. However, this can only remove the small copper particles that originate from the milling of conductor foil, since the copper of the plating is in the same size as the cathode coating material.

3.5 Zig-Zag air classifier products

The last process step of the performed mechanical recycling scheme (Fig. 1) is an air flow sorting using a Zig-Zag air classifier. To finally separate the decoated electrodes from each other and to generate Al- and Cu-metal concentrates another air flowing sorting with ZZAC is applied. In this stage, the aluminium has to be recovered to the light product as cathode concentrate and the copper to the heavy product as anode concentrate. As a high amount of the separator foil is still contained in the electrode foil product, either as uncoated separator foil or as coated separator foil (Fig. 2a), the possibility of introducing a third product was investigated. At 2 m/s (Kaas, Wilke et al. 2024) the entirely decoated separator foil showed a

recovery from 64% (P2-PTC) to 92% (C3 IPR) to the separator product. The PTC cells showed a better recovery of separator compared to the IPR cells. However, after the sorting the separator still makes up a share of up to 10% (P2 PTC) in the cathode foil fraction. Challenging is also the loss of cathode material to the separator product, which reached up to 11% (P2 IPR). Furthermore, the results showed that still coated separator foil remained in the cathode concentrate e.g., the share of coated separator foil for C3 IPR was 29% and for P2 IPR 68%. Even in the anode fraction for P2 IPR coated separator foil was found. In summary, it was not feasible to sort all coated and non-coated separator particles to an individual product. Therefore, it was chosen to stay with the conventional process design (Rothermel, Winter et al. 2018, Wuschke 2018), generating two products of cathode and anode concentrate by using a cut velocity of 4.7 m/s in the ZZAC.

Regarding the recovery of the aluminium into the cathode concentrate no clear differences between the different discharge levels are observed as can be seen in Figure 7c. Therefore, it can be concluded that also the mass of aluminium does not vary significantly between the PTC and IPR levels of a given cell type. However, disparities in aluminium recovery are evident when comparing C3 with prismatic cells. Possible causes for this are explained in (Kaas, Wilke et al. 2024), where the authors conclude that the narrower particle size distribution and more spherical shape of the foil particles could contribute to the lower recovery. Although the recovery of aluminium is similar for PTC and IPR cells, differences for the mass distribution are revealed. The main difference addresses the mass fraction of coated separator foil in the products. As this component could not be removed, the share in the IPR cells makes up $w_{\text{coated separator,cathode}}$ = 6% (P6 IPR) to $w_{\text{coated separator,cathode}}$ = 64% (P2 IPR). Due to the higher differences of coated separator foil in the individual fractions, the comparison of the other components is more challenging. Comparing the mass fractions of the anode in the cathode concentrate, it becomes clear that the discharge levels of P1 and C3 only differ slightly. A different result can be seen for P2 and P6. In these cases, the amount of smaller copper particles in the cathode concentrate is higher than for P1 and C3. This is supported by the lower recovery rates of copper for the anode concentrate (Fig. 7c).

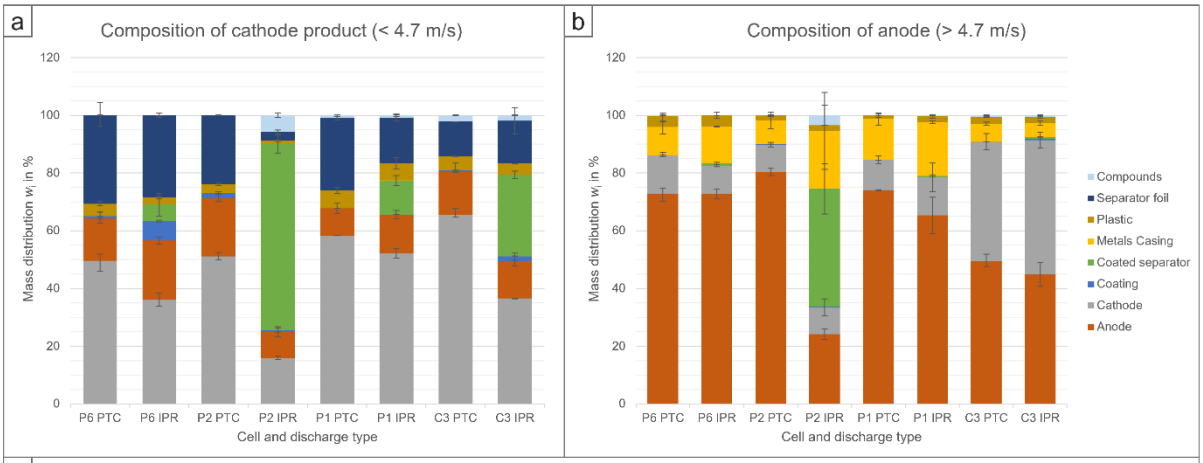

c

	P6		P2		P1		C3	
	PTC	IPR	PTC	IPR	PTC	IPR	PTC	IPR
$R_{c,Al}$ to cathode product	93,5	96,1	94,2	94,5	96,9	97,2	54,9	48,7
$R_{c,Cu}$ to anode product	95,2	79,3	91,7	61,7	97,3	94,3	97,2	93,7

Figure 7: Composition of the ZZAC products for (a) cathode product and (b) anode product together with (c) the recovery rates of Cu and Al for the investigated cells and discharge levels.

As displayed in Figure 7c, differences between IPR and PTC for the copper recovery in the anode concentrate range from 3% (P1) to 30% (P2). As already mentioned, this difference is attributed to the transfer of the smaller copper particles into the light product. The smaller particles result from the weakened copper foil due to the corrosion and ion transfer. This is also supported by the lower share of copper in the IPR anode concentrate compared to the PTC cells. Furthermore, the composition of P2 IPR stands out. The composition is mainly influenced by the coated separator foil. Most of the coated separator particles in the anode concentrate are larger in comparison to the smaller particles in the cathode concentrate. In combination with the higher share of coating on the separator foil in comparison to the other IPR cells, the settling velocity required increases. Therefore, the probability of a transfer to the heavier fraction is higher for these coated separator particles. Furthermore, C3 shows a higher share of cathode in the anode fraction, resulting from the low recovery rate to the cathode concentrate (Fig. 7a).

It can be concluded that the sorting process is mainly influenced and disturbed by the coated separator foil and the weakened copper current collector foils. Other plastics, such as the blank separator foil and thinner plastic foils also contaminate the concentrates, especially the cathode concentrate. Since the coated separator foil cannot be completely recovered as a separate product through another air flow sorting, a prior thermal treatment should be considered to decompose the separator and recover the active material. The temperature regime should be selected so that the binders are also decomposed in order to avoid unwanted side reactions, for example higher adhesion of the cathode coating to the current collector foil (Hanisch, Loellhoeffel et al. 2015). It is also useful for further processing, as the binders have

to be removed for flotation, for example. However, this is not the optimum solution as there are too many side effects: increased proportion of pyrolysis coke, higher energy consumption and possible aluminium oxidation. Integrating this thermal treatment upstream of the second sieving step (Fig. 1) could effectively recover the coating material into the black mass. In cases where separator foils are only coated to a certain extent like for P2 IPR, a thermal treatment of the cathode concentrate alone could be feasible to limit the mass of heated material and reduce emissions. Due to the problems outlined above, further research is needed to find ways of reducing the adhesion between the separator foil and the active material.

Conclusion and outlook

This study aims to evaluate the influence of depth of discharge of battery cells, which are processed with a characteristic mechanical recycling process (TU Bergakademie Freiberg), which is a characteristic mechanical recycling strategy. Therefore, four different LIB types were overdischarged (PTC) and discharged into pole reversal (IPR).

By subjecting the electrode fraction of the first part of the recycling process (Kaas, Wilke et al. 2023) to a further crushing step to increase the liberation and to support the decoating of the electrode foils, the liberation for PTC and IPR cells reached 94-99%. The high stress of the second comminution resulted in a decoating of the coated separator foils and liberation of compounds. Analysis showed that, next to the active material, copper deposits are also present on the coated separator foil. This means that further copper impurities are also introduced into the black mass fraction, which have to be dealt with by increasing the effort involved in hydrometallurgy. Despite the intensive mechanical stress, however, it is not possible to remove the plated copper layer from the active material. Therefore, a more detailed analysis of the particle behaviour inside the impact mill should be investigated.

The presence of copper deposits on both the separator foil and the active material on the cathode side lead to a shift of the copper yield to the black mass in the NMC cells of the IPR levels. However, the necessary recovery rate of the copper of 95% could also not be achieved with PTC cells only by the amount lost in the casing and anode fraction. This underscores the necessity of treating the black mass.

Concerning the additional recovery requirements of Ni, Co and Li, only P2 PTC was able to achieve these. In terms of the discharge depths, it can be assumed that the adhesion of active material to the separator caused a reduced recovery. In the cases of PTC and IPR cells, it is assumed that the mechanical stress is too low, so that the aluminium particles contain further residual coating. More intensive stress could lead to further decoating. However, this would be associated with higher copper contamination, especially for the cells with IPR level. The

structure of the anode foils analysed by AFM indicates a decrease in structural stability, likely due to corrosion and the partial ionisation of the copper atoms leading to changes in layer thickness.

When processing the foil mixture and analysing the sorting products after the zig-zag classifier, it becomes evident that the main difference in the separation behaviour is due to the coated separator foil which is still present. This component has a significant influence on the composition of the products. However, prior separation of the coated separator at lower air speeds showed no improvement. Hence, there is a need to explore alternative treatments for the remaining coated separator.

In summary, it can be said that the mechanical recycling process requires a redesign to react on the changes of material properties of the batteries due to the influence of discharge. The sifting step, which separates the separator into its own fraction shows no added value and reduces the recovery of the cathode components, as other components such as aluminium particles are discharged instead of the separator foil. In order to recover the active material from the coated separator film, higher stresses need to be applied in the shredding step or the material can be treated by pyrolysis.

Acknowledgement

The authors would like to thank Lakshmanrao Pentela, Jasmine Kavitha and Shreyan Mudgil for their support in manual sorting. The authors would like to thank Dr. Gert Schmidt of the Institute of Ceramics, Refractories and Composite Materials for performing the SEM imaging. Special thanks to Dr. Lisa Ditscherlein for carrying out the AFM measurements and Jan Nicklas for the plotting of the AFM data. Thanks, as well to Yvonne Volkmar and Annett Kästner for the black mass analysis. At last, the authors want to thank the technical and scientific staff of the Institute of Mechanical Process Engineering and Mineral Processing.

Funding

This research was funded by the German Federal Ministry for Education and Research (BMBF), as well as the Projektträger Jülich (PTJ), with the projects DIGISORT (Digitalisation of mechanical sorting processes in mechanical battery recycling) 03XP0337 and LOWVOLMON (Monitoring of low-volatile electrolytes in the mechanical recycling process chain) 03XP0354 within the competence cluster for battery recycling (greenBatt).

Author contribution

A.K. and C.W. developed the idea and the content of the report; A.K. and C.W conducted the experiments, analyzed the resulting data and results; A.K. wrote the article; A.V. made the SEM-EDX pictures and discussed the results with A.K and C.W.; U.A.P. and A.V. revised the article and improved both the presentation of the results and the structure of the chapters; everything took place under the supervision of U.A.P. All authors have read and agreed to the published version of the manuscript.

Symbols and Indices

Latin Symbol	Meaning	Unit
c	Concentration	%
m	Mass	g
w	Mass distribution	%
w_m	Specific stress energy	kWh/t
R	Recovery	%
Y	Yield	%

Indice	Meaning
BM	Black Mass
c	concentrate
i	Component
Me	Metal

References

Doose, S., et al. (2021). "Challenges in ecofriendly battery recycling and closed material cycles: a perspective on future lithium battery generations." Metals **11**(2): 291.

EU (2023). REGULATION (EU) 2023/1542 OF THE EUROPEAN PARLIAMENT AND OF THE COUNCIL of 12 July 2023 concerning batteries and waste batteries, amending Directive 2008/98/EC and Regulation (EU) 2019/1020 and repealing Directive 2006/66/EC. Brussels, Official Journal of the European Union.

Fear, C., et al. (2018). "Elucidating copper dissolution phenomenon in Li-ion cells under overdischarge extremes." Journal of the Electrochemical Society **165**(9): A1639.

Feng, X., et al. (2018). "Thermal runaway mechanism of lithium ion battery for electric vehicles: A review." Energy storage materials **10**: 246-267.

Flügel, M., et al. (2021). "Cu dissolution during over-discharge of Li-ion cells to 0 V: a post-mortem study." Journal of the Electrochemical Society **168**(2): 020506.

Fuentevilla, D., et al. (2015). "Quantifying the impact of overdischarge on large format lithium-ion cells." ECS Transactions **69**(20): 1.

Gräfensteiner, P., et al. (2024). "An AFM-based approach for quantification of guest particle deformation during mechano-fusion." Powder technology **434**: 119293.

Hanisch, C., et al. (2015). "Recycling of lithium-ion batteries: a novel method to separate coating and foil of electrodes." Journal of cleaner production **108**: 301-311.

Hashimoto, M., et al. (2015). "Mechanism of gas generation in lithium ion batteries by overdischarge." ECS Transactions **69**(20): 17.

He, H., et al. (2013). "Failure investigation of LiFePO4 cells in over-discharge conditions." Journal of the Electrochemical Society **160**(6): A793.

Hendricks, C. E., et al. (2020). "Copper dissolution in overdischarged lithium-ion cells: X-ray photoelectron spectroscopy and X-ray absorption fine structure analysis." Journal of the Electrochemical Society **167**(9): 090501.

Juarez-Robles, D., et al. (2020). "Degradation-safety analytics in lithium-ion cells: Part I. Aging under charge/discharge cycling." Journal of the Electrochemical Society **167**(16): 160510.

Kaas, A., et al. (2024). "Supplementary information to the publication “Evaluating the influence of discharge depths of lithium-ion batteries on the mechanical recycling process"." 2024, from https://opara.zih.tu-dresden.de/xmlui/handle/123456789/6113.

Kaas, A., et al. (2024). "Modelling the Sorting of Lithium-Ion Battery Components in a Zig-Zag Air Classifier." Metals **14**(3): 269.

Kaas, A., et al. (2023). "Influence of different discharge levels on the mechanical recycling efficiency of lithium-ion batteries." Waste Management **172**: 1-10.

Kasnatscheew, J., et al. (2017). "Lithium ion battery cells under abusive discharge conditions: Electrode potential development and interactions between positive and negative electrode." Journal of Power Sources **362**: 278-282.

Korthauer, R. (2013). Handbuch lithium-ionen-batterien, Springer.

Li, W., et al. (2021). "Treatment of electric vehicle battery waste in China: A review of existing policies." Journal of Environmental Engineering and Landscape Management **29**(2): 111-122.

Maleki, H. and J. N. Howard (2006). "Effects of overdischarge on performance and thermal stability of a Li-ion cell." Journal of Power Sources **160**(2): 1395-1402.

Neef, C., et al. (2021). "Recycling von Lithium-Ionen-Batterien: Chancen und Herausforderungen für den Maschinen-und Anlagenbau."

Or, T., et al. (2020). "Recycling of mixed cathode lithium-ion batteries for electric vehicles: Current status and future outlook." Carbon Energy **2**(1): 6-43.

Park, S., et al. (2019). "The effect of Fe as an impurity element for sustainable resynthesis of Li [Ni1/3Co1/3Mn1/3] O2 cathode material from spent lithium-ion batteries." Electrochimica Acta **296**: 814-822.

Peng, C., et al. (2020). "Role of impurity copper in Li-ion battery recycling to LiCoO2 cathode materials." Journal of Power Sources **450**: 227630.

Rothermel, S., et al. (2018). Recycling of Lithium-Ion Batteries: The LithoRec Way. Recycling of Lithium-Ion Batteries: The LithoRec Way. K. A and J. Diekmann. New York, Springer**:** 1-31.

Schmaltz, T. (2023). "Recycling of lithium-ion batteries will increase strongly in Europe." Retrieved 08/29, 2023, from https://www.isi.fraunhofer.de/en/blog/themen/batterie-update/recycling-lithium-ionen-batterien-europa-starke-zunahme-2030-2040.html.

Shi, C., et al. (2016). "A high-temperature stable ceramic-coated separator prepared with polyimide binder/Al2O3 particles for lithium-ion batteries." Journal of Membrane Science **517**: 91-99.

Sommerville, R., et al. (2020). "A review of physical processes used in the safe recycling of lithium ion batteries." Sustainable Materials and Technologies **25**: e00197.

Wang, D., et al. (2020). "Effects of overdischarge rate on thermal runaway of NCM811 Li-ion batteries." Energies **13**(15): 3885.

Wang, W., et al. (2019). "Hydrometallurgical preparation of lithium carbonate from lithium-rich electrolyte." Hydrometallurgy **185**: 88-92.

Wang, Y., et al. (2023). "Challenges and opportunities to mitigate the catastrophic thermal runaway of high-energy batteries." Advanced Energy Materials **13**(15): 2203841.

Werner, D., et al. (2020). "Recycling chain for spent lithium-ion batteries." Metals **10**(3): 316.

Wilke, C., et al. (2023). "Influence of the Cell Type on the Physical Processes of the Mechanical Recycling of Automotive Lithium-Ion Batteries." Metals **13**(11): 1901.

Wilke, C., et al. (2023). "Influence of the Crusher Settings and a Thermal Pre-Treatment on the Properties of the Fine Fraction (Black Mass) from Mechanical Lithium-Ion Battery Recycling." Batteries **9**(10): 514.

Windisch-Kern, S., et al. (2022). "Recycling chains for lithium-ion batteries: A critical examination of current challenges, opportunities and process dependencies." Waste Management **138**: 125-139.

Wu, C., et al. (2015). Research on overcharge and overdischarge effect on lithium-ion batteries. 2015 IEEE Vehicle Power and Propulsion Conference (VPPC), IEEE.

Wu, L., et al. (2018). "In situ temperature evolution and failure mechanisms of LiNi0. 33Mn0. 33Co0. 33O2 cell under over-discharge conditions." Journal of the Electrochemical Society **165**(10): A2162.

Wuschke, L. (2018). Mechanische Aufbereitung von Lithium-Ionen-Batteriezellen. Freiberg, Technische Universität Bergakademie Freiberg.

Wuschke, L., et al. (2019). "Crushing of large Li-ion battery cells." Waste Management **85**: 317-326.

Xiao, Y., et al. (2013). "Influence of Cu substrate topography on the growth morphology of chemical vapour deposited graphene." Carbon **65**: 7-12.

Yung, K. C., et al. (2007). "Surface characterization of pre-treated copper foil used for PCB lamination." Journal of adhesion science and technology **21**(5-6): 363-377.

Zhao, C., et al. (2019). "Lithium carbonate recovery from lithium-containing solution by ultrasound assisted precipitation." Ultrasonics sonochemistry **52**: 484-492.

Zhao, S., et al. (2019). Recycling technology and principle of spent lithium-ion battery. Recycling of spent Lithium-ion batteries, Springer**:** 1-26.